Council for Energy and Minerals, Houston, TX, 1987), pp. 403–448.
15. J. K. Crouch and J. Suppe, *Geol. Soc. Am. Bull.* **105**, 1415 (1993).
16. H. Zhou, *J. Geophys. Res.* **99**, 15,439 (1994); *Eos* **75**, 483 (abstr.) (1994). This technique properly accounts for three-dimensional crustal and upper-mantle seismic velocity heterogeneities while determining hypocenters. The SCSN earthquake catalog hypocenters are found with a one-dimensional velocity model. However, the general features of the hypocenter depth patterns we discuss here are apparent in the best quality hypocenters in the SCSN earthquake catalog.
17. The earthquakes used here were selected to have small location errors as determined by the SCSN catalog and to have been recorded on at least 10 stations used for relocations. These selection parameters exclude earthquakes that are poorly constrained as a result of the low station density near the periphery of the SCSN. In the central part of the SCSN that we examine here, the hypocentral errors are <1 km (*16*).
18. H. Magistrale and C. Sanders, *J. Geophys. Res.* **101**, 3031 (1996).
19. S. M. Green, thesis, University of California, Los Angeles (1983); E. J. Corbett, thesis, California Institute of Technology (1984); T. H. Webb and H. Kanamori, *Bull. Seismol. Soc. Am.* **75**, 737 (1985); C. Nicholson, L. Seeber, P. Williams, L. R. Sykes, *J. Geophys. Res.* **91**, 4891 (1986); L. M. Jones, E. Hauksson, H. Qian, *Seismol. Res. Lett.* (abstr.) **64**, 22 (1993).
20. R. H. Sibson, *J. Geophys. Res.* **89**, 5791 (1984); R. Meissner and J. Strehlau, *Tectonics* **1**, 73 (1982); S. T. Tse and J. R. Rice, *J. Geophys. Res.* **91**, 9452 (1986); C. H. Scholz, *The Mechanics of Earthquakes and Faulting* (Cambridge Univ. Press, New York, 1990).
21. R. H. Sibson, *Bull. Seismol. Soc. Am.* **72**, 151 (1982).
22. J. C. Matti, D. M. Morton, B. F. Cox, *U.S. Geol. Surv. Open-File Rep. 85-355* (1985).
23. E. S. Larsen, *Geol. Soc. Am. Mem. 29* (1948).
24. D. A. Pickett and J. B. Saleeby, *J. Geophys. Res.* **98**, 609 (1993).
25. R. V. Sharp, *Geol. Soc. Am. Bull.* **78**, 705 (1967).
26. J. Dolan *et al.*, *Science* **267**, 199 (1995).
27. Working Group on California Earthquake Probabilities, *Bull. Seismol. Soc. Am.* **85**, 379 (1995).
28. In addition to the events shown in Fig. 3, we also checked the magnitude (*M*) 6.0 1987 Whittier Narrows, *M* 5.0 1988 Pasadena, *M* 5.0 1989 Malibu, *M* 4.6 1988 and *M* 5.2 1990 Upland, *M* 5.6 1991 Sierra Madre, and *M* 6.1 1992 Joshua Tree earthquakes. Some of these earthquakes occurred in areas underlain by schists and some in areas underlain by other kinds of rock; in every case the main shock–aftershock sequence had the same maximum depth as the local background seismicity. In some cases (for example, the Landers area in Fig. 3) the background seismicity was sparse but adequately defined the maximum depth.
29. C. M. Schiffries and T. L. Henyey, *Geotimes* **39**, 4 (1994); D. D. Jackson, *Seismol. Res. Lett.* **67**, 3 (1996).
30. C. E. Jacobson, *J. Geophys. Res.* **95**, 509 (1990).
31. To map the subsurface distribution of the Pelona, Orocopia, and Rand schists, we accept the conclusion of (*1*) that continuous schist is present under the western Mojave. Models of the emplacement of the schist protoliths also imply regional continuity of the schists (*1–7*), and seismic reflection surveys image the schists as continuous features extending beyond the survey areas (*8–11*). Constraints in the area of cross section A–A′ (Fig. 2) are from (*1, 7, 22*); cross section B–B′, from (*3, 32*); cross section C–C′, from (*3, 9, 32*); cross section D–D′, from (*11, 24*); and cross section E–E′, from L. T. Silver and J. A. Nourse, *Geol. Soc. Am. Abstr. Programs* **18**, 185 (abstr.) (1986); J. B. Saleeby, L. T. Silver, D. J. Wood, P. E. Malin, *ibid.* **25**, 141 (abstr.) (1993); and L. T. Silver, *ibid.* p. 147 (abstr.). Also, the southern Sierra Nevada Mountains are structurally continuous with the Tehachapi Mountains [J. B. Saleeby, D. B. Sams, R. K. Kistler, *J. Geophys. Res.* **92**, 10,443 (1987)] where schist is present (*11, 24*). The subsurface distribution of the Catalina schist is from (*13–15*); T. L. Wright, in *Active Margin Basins, Am. Assoc. Pet. Geol. Mem. 52*, K. T. Biddle, Ed. (American Association of Petroleum Geologists, Tulsa, OK, 1991), pp. 35–134; and J. E. Schoellhamer and A. O. Woodford, *U.S. Geol. Surv. Oil Gas Invest. Map OM-117* (1951). There is minor disagreement about the eastern limit of the Catalina Schist under part of the Los Angeles basin (*14, 15*); here we follow (*14*).
32. A. P. Barth, C. E. Jacobson, D. J. May, in *Geological Excursions in Southern California and Mexico*, M. J. Walawender and B. B. Hanan, Eds. (Department of Geological Sciences, San Diego State University, San Diego, CA, 1991), pp. 186–198.
33. We thank L. Silver for providing a compilation of the subsurface distribution of the schists; C. Sanders for clarifying ideas; and S. Day, E. Frost, and G. Girty for reviews of the manuscript. Supported in part by NSF grant EAR-9218704 to H.Z.

26 February 1996; accepted 29 May 1996

Mechanism of Phreatic Eruptions at Aso Volcano Inferred from Near-Field Broadband Seismic Observations

Satoshi Kaneshima,* Hitoshi Kawakatsu,† Hirotoshi Matsubayashi, Yasuaki Sudo, Tomoki Tsutsui, Takao Ohminato, Hisao Ito, Koichi Uhira, Hitoshi Yamasato, Jun Oikawa, Minoru Takeo, Takashi Iidaka

Broadband seismometers deployed at Aso volcano in Japan have detected a hydrothermal reservoir 1 to 1.5 kilometers beneath the crater that is continually resonating with periods as long as 15 seconds. When phreatic eruptions are observed, broadband seismograms elucidate a dynamic interplay between the reservoir and discharging flow along the conduit: gradual pressurization and long-period (~20 seconds) pulsations of the reservoir during the 100 to 200 seconds before the initiation of the discharge, followed by gradual deflation of the reservoir concurrent with the discharging flow. The hydrothermal reservoir, where water and heat from the deeper magma chamber probably interact, appears to help control the surface activity at Aso volcano.

The activity of volcanoes has been conventionally monitored with short-period seismometers (>1 Hz) (*1*) and with geodetic instruments including strain- and tilt-meters (*2*). Short-period records of volcanic earthquakes and tremors describe stress accumulation around magma chambers or fluid flow through conduits, whereas strain- and tilt-meters mainly record quasi-static deformation associated with slower responses of pressure sources, such as a magma chamber. Ground motions in the frequency range from 0.01 to 1 Hz, which has not been widely monitored, may elucidate the detailed structure of pressure sources and the dynamics of mass advection during an eruption (*3*).

S. Kaneshima, Department of Earth and Planetary Physics, Faculty of Science, University of Tokyo, Bunkyo-ku, Tokyo 113, Japan.
H. Kawakatsu, H. Matsubayashi, J. Oikawa, M. Takeo, T. Iidaka, Earthquake Research Institute, University of Tokyo, Bunkyo-ku, Tokyo 113 Japan.
Y. Sudo and T. Tsutsui, Aso Volcanological Laboratory, Faculty of Science, Kyoto University, Aso, Kumamoto 869-14, Japan.
T. Ohminato and H. Ito, Geological Survey of Japan, Tsukuba, Ibaraki 305, Japan.
K. Uhira, Japan Meteorological Agency, Chiyoda-ku, Tokyo 110, Japan.
H. Yamasato, Meteorological Research Institute, Tsukuba, Ibaraki 305, Japan.

*Currently on leave at Department of Geology, University of Bristol, Bristol BS8 1RJ, UK.
†To whom correspondence should be addressed. E-mail: hitoshi@eri.u-tokyo.ac.jp

From April 1994 through March 1995, we operated 10 to 12 broadband, three-component velocity seismometers around Aso volcano in Japan (Fig. 1) (*4*). When Aso volcano was quiescent, that is, when there was a lack of major surface activity at the crater, our seismometers detected tremors with unusually long periods (~15 s) (*5, 6*) almost continuously throughout the 1 year of the experiment. A long-period tremor (LPT) consisted of a series of isolated wave packets with an amplitude of about 1 μm with a duration of about 30 s (Fig. 2). Amplitude spectra at three stations obtained by stacking many events showed that the dominant period of each LPT was about 15 s (Fig. 3). The observed spectra also showed other consistent long-period peaks at about 7.5, 5, and 3 s, which correspond to the second, third, and fifth overtones of the harmonic oscillation with a fundamental period of 15 s (Fig. 3). The presence of overtones indicates that the LPT was an oscillation of a resonator (*7*).

At most stations near the crater, the horizontal particle motions of LPTs in the 10- to 30-s bandpassed seismograms were rectilinear and pointed toward the crater. The particle motions in the radial plane showed that the incident angles of the LPTs observed at most stations around the crater ranged from about 35° to 70° (Fig. 4B). Assuming that

the source radiation is isotropic, the LPTs can be located with the use of wave form semblance analysis (8). The inferred point source of the LPTs, which best explains their particle motions as well as their relative arrival times, was a few hundred meters southwest of the crater at depths of 1 to 1.5 km (Fig. 4A). This area can be considered as the centroid location of moment release. The size of the source region was more difficult to estimate but appears to be smaller than 1 km in diameter, considering the pattern of the observed particle motions and amplitudes at the stations near the crater (9). The first motions of LPTs were usually polarized negatively and were often accompanied by short-period (~0.3 to 0.5 s) signals (*10*) (Fig. 2, B and C).

During our experiment, Aso volcano became intermittently active, and a number of phreatic eruptions—small eruptions of mud, water, and steam—were observed (*11*) (Fig. 5). A good correlation was observed between the occurrence of short-period (~0.3 to 0.5 s) tremors [SPTs (*12*)] and the discharge of gas, water, and fragmented rocks (hereafter called "fluid-rock mixture" for simplicity) from the crater lake. We assumed that a SPT was caused by a fluid-rock mixture moving along a conduit connected to the crater (*13*). We took the duration of the discharge of the fluid-rock mixture to be the SPT duration and measured the energy of an eruption by integrating squared amplitudes of velocity seismograms over the duration of discharge. There is a clear tendency for longer eruptions to have larger SPT amplitudes (*14*). On the basis of their duration, or nearly equivalently their energy, phreatic eruptions were classified into two groups: one with durations less than 50 s (small eruptions), and the other with durations exceeding 50 s (large eruptions).

Small eruptions had a characteristic pattern of excitation of SPTs: a small initial tremor of 15 to 20 s, rapid increase of amplitude, roughly steady continuation at similar amplitudes for 20 to 50 s, and a rather sudden cease of tremor (Fig. 5A). Long-period (~15 s) signals with amplitudes that exceeded those of LPT were rarely observed (Fig. 5A).

Large eruptions, while sharing SPT features with the small eruptions, show spectacular broadband features (Fig. 5B). (i) A very long-period displacement (VLPD), corresponding to slow inflation in the source region, preceded mass discharge by 50 to 150 s. (ii) Long-period pulses (LPPs) with a dominant period of 15 to 20 s predominantly positively polarized were superimposed on the VLPD during the inflation. (iii) As the inflation approached its maximum, SPT (dominant period, 0.3 to 0.5 s) with small amplitude (~1 μm) began, and the LPP's downswing motion relative to upswing motion became larger. (iv) About 15 to 20 s after its onset, the amplitude of the SPT increased rapidly (>10 μm) during a downswing of LPP. This increase was approximately synchronized with the air-pressure perturbation recorded by a microbarograph (Fig. 1) that corresponded to the time of the onset of mass discharge from the crater lake. The VLPD turned into deflation, and the excitation of LPP was suppressed. (v) The duration of the SPT and that of the deflating VLPD were 100 to 200 s. The SPT remained nearly stationary during the deflation and rather abruptly ceased concurrent with the end of deflation.

The observed spectra of LPPs showed a large peak around 15 to 20 s. In this period range, LPPs had similar particle motions to those of LPTs (Fig. 4B). Correspondingly, LPPs were located by the semblance method to almost the same source region as the LPTs (Fig. 4A). As for the VLPD, it may result from a gradual increase in fluid pressure beneath the crater; we estimated the location of the pressure source as well as the magnitude of the pressure change using a spherical pressure source model (*15*). The source location that fits the observed displacements best is 300 m west of and 1 to 1.5 km below the crater (Fig. 4A), close to the source of the LPT (*16*). We thus infer that the source regions of LPTs, LPPs, and VLPD are the same. This source region constantly vibrates, emitting LPTs even when the volcano is inactive, and acts as a pressure source of LPP and VLPD for large phreatic eruptions.

There are several pieces of evidence that suggest that the source region of the long-period signals—LPT, LPP, and VLPD—is not a magma chamber. First, the source region is shallow (1 to 1.5 km below the crater). Second, Aso volcano is in a relatively quiet period (the last magmatic eruption occurred in 1990). Third, the surface temperature of the crater lake is only 70°C, and the water of the lake has not evaporated. The presence of ample water, as well as a

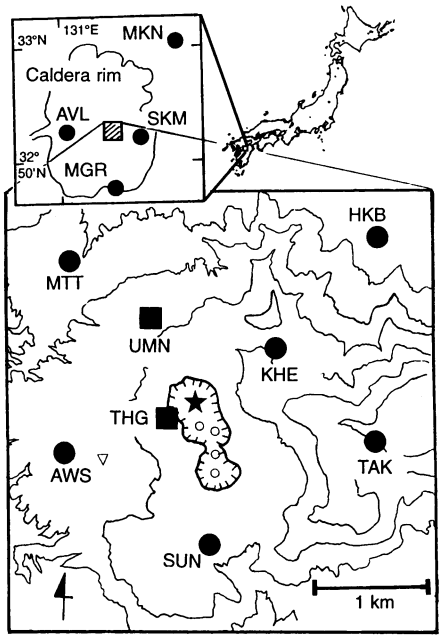

Fig. 1. Stations around Aso volcano. Aso is an andesitic volcano located in the middle of Kyushu, Japan. We installed 10 broadband three-component velocity seismometers with a free period of 120 s (STS2) or 30 s (CMG3) (filled circles). In November 1994, two other seismometers (CMG3, with a 100-s free period) were also temporarily deployed near the crater for 8 days to improve the azimuth and distance coverage of stations relative to the crater (filled squares). Eight of the 12 stations are around the Nakadake first crater (star) on the central cone (shaded square in inset). The other four stations are near the outer rim of the caldera (solid line in inset). A north-by-northwest–south-by-southeast trending chain of older craters are indicated by small open circles. Topography near the craters is shown by contours at an interval of 100 m. A microbarograph was installed 300 m east of station AWS (open triangle).

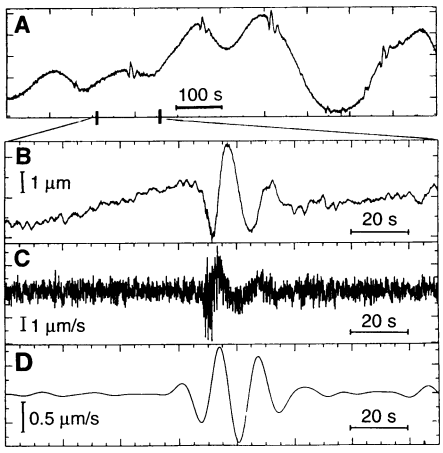

Fig. 2. (**A**) Vertical-displacement seismogram of LPT for a period of 800 s (23 November 1994). (**B**) Vertical displacement, (**C**) velocity, and (**D**) 10- to 30-s band-passed seismograms of LPT (23 November 1994) for a period of 150 s.

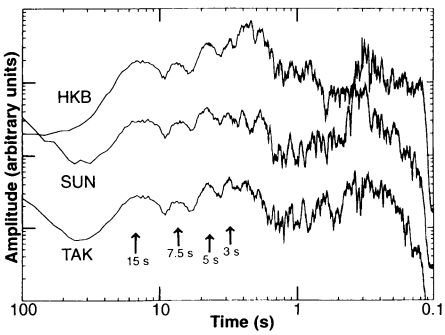

Fig. 3. Amplitude spectrum of LPT for three stations obtained by the stacking of 24 hours of data from 27 July 1994.

system that can quickly circulate the water below the crater, was suggested by the quick changes in geomagnetic field associated with the activity of Aso volcano (*17*). It seems more plausible that the source region is a hydrothermal reservoir in an aquifer that contains cracks or fractures filled with gas, water, and fragmented rocks (Fig. 6).

We equate the hydrothermal reservoir with the source region of LPT, LPP, and VLPD and explain the essential features of the observed broadband seismograms. Heat is gradually transported upward to the surface from a deep-seated magma chamber in the form of high-temperature liquid or gas even during quiet stages of Aso volcano. The hydrothermal reservoir buffers such upward heat transport. The pressure in the hydrothermal reservoir is sustained by the heat flow from below and by gradual leakage of the fluid-rock mixture upward to the bottom of the crater lake. Sporadic and rapid leakage of fluid-rock mixture through fractures above the hydrothermal reservoir generates SPT and causes the aquifer to shrink and resonate, which results in LPT (Fig. 2). The seismic source region is recharged by the continuous upward transport of magmatic heat from depth.

A phreatic eruption could be triggered by a pressure release due to, for instance, fracture of impermeable "cap rocks" near the crater (*18*, *19*). The durations of small initial SPT of phreatic eruptions of Aso volcano were nearly constant around 15 to 20 s and rarely exceeded 25 s regardless of the eruption size. Records of a microbarograph (Fig. 1) showed that discharge flow from the crater tended to start not at the beginning of the small initial SPT but when the SPT amplitudes rapidly increased (Fig. 5). Once the fluid-rock mixture starts ascending, it could be accelerated to near its sound velocity. If the sound velocity is 100 m/s (*19*, *20*), a fluid-rock mixture flow that starts ascending from a depth near 1 km will reach the bottom of the crater within 10 to 20 s. This time interval corresponds to the duration of the initial small SPT. The constancy of the duration of the initial SPT would mean that cap rocks nearly immediately break when pressure perturbations accompanying the conduit fluid reaches this point. A simple application of gas dynamics to the flow along the vent of the conduit predicts that the flow continues for 40 to 50 s (*21*).

For small eruptions, there are few LPPs, which suggests that the flow does not ascend directly from the hydrothermal reservoir. For large phreatic eruptions, the observation of LPPs and VLPD indicates that the reservoir is more dynamically involved in the eruption process. A VLPD possibly corresponds to a gradual pressurization and inflation of the hydrothermal reservoir because of increases of the heat injection rate from a magma chamber below. Positively polarized LPPs may represent more rapid increase of the pressure in the reservoir. It is possible that LPPs are associated with injection of high-temperature materials such as magma or volcanic gas from below, which will touch and explosively vaporize ground water in the reservoir. When the inflation approaches a threshold (*16*), fluid-rock mixture begins a permeable flow out of the hydrothermal reservoir and eventually up to the crater; this discharge flow causes the initial small SPT, deflates the reservoir, and excites a negatively polarized LPP. Once the conduit flow to the crater has developed, the discharge flow of fluid-rock mixture becomes roughly stable, exciting SPT of larger amplitude. During the discharge, the reservoir pressure decreases and deflating VLPD occurs, but the excitation of LPP is suppressed. The cessation of SPT corresponds to the end of the discharge, and the source region is deflated back to a static level (*22*).

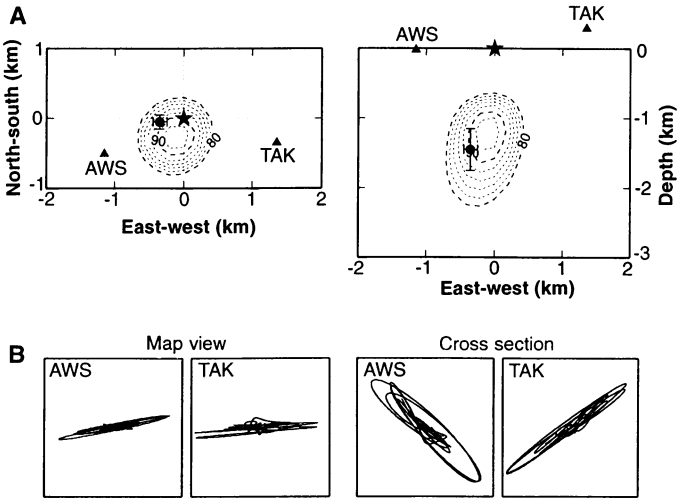

Fig. 4. (**A**) Estimated locations of LPT and LPP from a three-dimensional semblance method. Contours of semblance value above 0.8 with an interval of 2% are plotted in a map view and an east-west cross section. Bandpassed (10 to 30 s) three-component seismograms at five close-in stations (TAK, SUN, AWS, KHE, and HKB) were used for the analyses. Also plotted with error bars is the location of a typical VLPD source (closed circle) estimated by fitting the observed VLPD amplitudes with the Mogi model. A star indicates the location of the crater. (**B**) Particle motions of a typical LPT are projected on the planes of the same map view and east-west cross section as above. Wave forms in the frequency corresponding to the fundamental mode recorded at AWS and TAK on 7 June 1994 are shown.

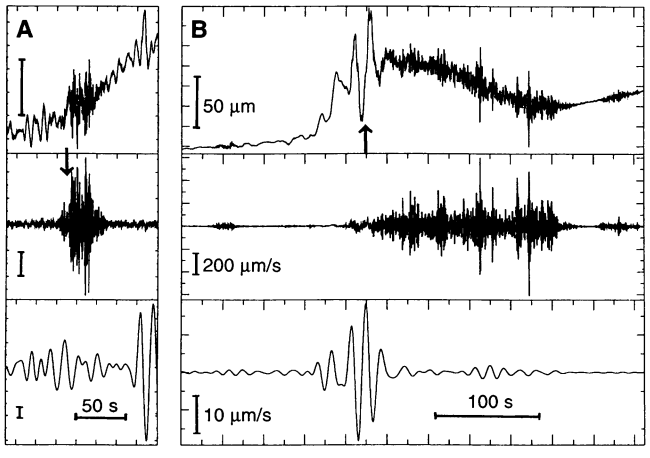

Fig. 5. (**A**) Small phreatic eruption on 18 September 1994 (20:25 GMT) observed at SUN. (top, vertical displacement; middle, velocity; bottom, bandpass 10 to 30 s). Arrow indicates the onset of the eruption derived by the arrival of air shock measured by a microbarograph (Fig. 1). This approximately corresponds to the rapid increase in the SPT amplitude. The initial SPT is defined as the tremor between its beginning and the rapid amplitude increase. Seismograms for each eruption at different close-in stations shared the same features but their amplitudes differed. Scale bars for each trace indicates amplitudes one order smaller than those of corresponding traces in (B): 5 μm, 20 μm/s, and 1 μm/s, respectively. (**B**) Large phreatic eruption on 15 September 1994 (10:21 GMT) recorded at TAK. Details are the same as (A), except for the size of the scale bars.

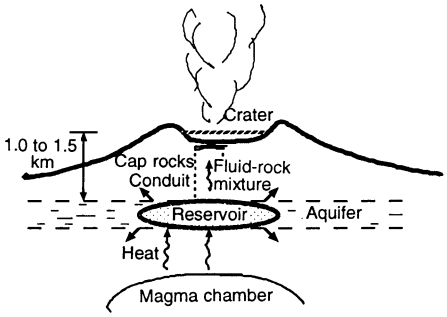

Fig. 6. Schematic view of the hydrothermal system associated with phreatic eruptions at Aso volcano.

REFERENCES AND NOTES

1. R. Y. Koyanagi *et al.*, *Volcanism in Hawaii* (Government Printing Office, Washington, DC, 1987), pp. 1221–1257.
2. K. Kamo and K. Ishihara, *Bull. Disaster Prev. Res. Inst.* **29B**, 1 (1986); A. T. Linde *et al.*, *Nature* **365**, 737 (1993).
3. So-called single-force models have been applied to explain long-period seismic wave forms attributable to such mass advection at different volcanoes of the world [H. Kanamori and J. W. Given, *J. Geophys. Res.* **87**, 5422 (1982); K. Uhira and M. Takeo, *ibid.* **99**, 17775 (1994)]. Recent advances in seismometry have now made such observations rather straightforward; portable equipment covering a wide frequency band (50 to 0.01 Hz) can be easily installed at volcanoes, and the broadband nature of volcanic activity is becoming increasingly clear [H. Kawakatsu *et al.*, *Geophys. Res. Lett.* **19**, 1959 (1992); T. Ohminato *et al.*, *Eos* **74**, 648 (1993); R. Dreier *et al.*, *Acta Vulcanol.* **5**, 165 (1994); S. Falsaperla *et al.*, *ibid.*, p. 173; J. Neuberg *et al.*, *Geophys Res. Lett.* **21**, 749 (1994); P. Hellweg *et al.*, *Eos* **75**, 313 (1994)].
4. Seismic signals were recorded continuously with portable data loggers either on digital tapes, hard disks, or magneto-optical disks, with a sampling rate of 20 Hz and dynamic range of either 16 or 24 bits. Recorder clocks were either locked with GPS (Global Positioning System) or adjusted by radio time signals, providing accurate enough timing for later analyses of long-period signals.
5. Disturbances commonly called long-period events at volcanoes are in the period range 0.2 to 2 s [B. J. Chouet, *Nature* **380**, 309 (1996)].
6. Long-period seismometers installed at the Aso volcano 60 years ago revealed the presence of long-period (3.5 to 7 s) volcanic tremors [K. Sassa, *Mem. Coll. Sci. Kyoto Univ. Ser. A* **18**, 255 (1935)]. The observation of long-period volcanic tremors has been repeatedly reported [M. Churei, *Bull. Volcanol. Soc. Jpn.* **30**, 71 (1985); T. Hashida, *ibid.* **35**, 323 (1990); H. Kawakatsu *et al.*, *Geophys. Res. Lett.* **21**, 1963 (1994)], but those observations have fallen short of unraveling their origin because of the limited number of instruments near the crater.
7. One of the possible mechanisms generating the LPT may be resonance of a vertical crack filled with fluid [B. J. Chouet, *J. Geophys. Res.* **91**, 13967 (1986); V. Ferrazzini and K. Aki, *ibid.* **92**, 9215 (1987)]. The presence of waves trapped in the crack that propagate with a phase velocity much slower than the sound velocity of the fluid—the so called "crack wave"—has been proposed. Consideration of the crack wave would greatly reduce the estimate of the size of the resonator.
8. N. Neidel and M. T. Tarner, *Geophysics* **36**, 483 (1971). To improve the resolution of source depth, we extended conventional single-component semblance analyses to three-component wave forms [H. Matsubayashi, thesis, Tokyo University (1995)].
9. Moment tensor inversion of LPT wave forms gives a best point source solution corresponding to a combination of isotropic expansion (contraction) and inflation (deflation) of a vertical crack aligned from north-northwest to south-southeast, parallel or subparallel to the chain of older craters (Fig. 1). A LPT source with a finite extent can be approximated by a summation of point sources. As long as we retain the above moment tensor solution throughout the source, LPT amplitudes at the stations located northeast or southwest of the crater (KHE and AWS) are greatly increased by putting point sources near these stations, and particle motions at these stations become too steep to match the observations, which may indicate that the effective extent of the LPT source does not exceed several hundred meters from the center of the crater.
10. S. Kikuchi, *Bull. Disaster Prev. Res. Inst.* **17B**, 1 (1974).
11. The meteorological station at Aso reported that the ash and smoke went up as high as 1 km when one of the eruptions took place at 06:31 (GMT) on 15 September. Shock waves were not reported for any of the eruptions. At the largest eruptions, ejecta of fragmented rocks ascended to a height of nearly 150 m above the crater lake, with corresponding initial velocities of the order of 50 m/s. The velocities of the steam that entrained those solid ejecta is bounded by the sound velocity in the atmosphere (330 m/s) and that of solid ejecta.
12. The presence of many different kinds of short-period tremors are known at Aso volcano (*6*), and here we specifically call the kind associated with phreatic eruptions SPT. Note also that the short-period tremors that we call SPTs here may be referred to as long-period events or tremors at other volcanoes (*5*).
13. G. S. Steinberg and A. S. Seinberg, *J. Geophys. Res.* **80**, 1600 (1975).
14. Larger eruptions tend to excite larger pressure waves at the time of mass ejection, which is recorded at a microbarograph near the crater (Fig.1), although the correlation is rather weak.
15. K. Mogi, *Bull. Earthquake Res. Inst.* **36**, 99 (1958).
16. If we assume a radius of 200 (± 92) m for the spherical source, the pressure change is on the order of 0.1 (± 1.0) MPa for typical large eruptions, which amounts to about 0.5 (± 5.0)% of the lithostatic pressure (20 MPa).
17. Y. Tanaka, *J. Volcanol. Geotherm. Res.* **2**, 319 (1993).
18. K. Wohletz and G. Heiken, *Volcanology and Geothermal Energy* (Univ. of California Press, Berkeley, 1992).
19. S. W. Kiefer and B. Sturtevant, *J. Geophys. Res.* **89**, 8523 (1984).
20. S. W. Kiefer, *ibid.* **82**, 2895 (1977).
21. The durations of the small eruptions at Aso volcano may be interpreted by the "choked flow" model of the conduit flow of fluid-rock mixture (*19*). Suppose that the conduit pressure is lithostatic at a depth near 1000 m (~20 MPa), where fluid-rock mixture starts ascending (*18*), and the mixture behaves as ideal gas. After 10 to 20 s of initial fluid-rock mixture flow to the bottom of cap rocks below the crater, there would be a good connection of fluid-rock mixture from the starting depth to the cap rocks, building up an excess pressure on the order of 10 MPa below the cap rocks (*18, 23*). When the cap rocks finally fracture, the explosive discharge of a large volume of fluid-rock mixture into the atmosphere occurs. The flow would quickly reach a nearly steady state and be choked at the vent of the conduit with a velocity of sound. This flow may be approximated as a one-dimensional steady flow out of a tank (which is the conduit in this case). The choked flow will be sustained until the pressure at the orifice decreases to the atmospheric value (0.1 MPa) (*19*), corresponding to the tank pressure P_t about 0.18 MPa (for a γ, isentropic exponent, of 1.4). The duration of choked flow is described as $Vt(\gamma,P_0/P_t)/Ac_0$, where V, A, and c_0 are, respectively, tank volume, area of the orifice, and the initial sound velocity in the tank. The constant $t(\gamma,P_0/P_t)$ depends on γ and P_0/P_t, where P_0/P_t is the ratio of initial and final tank pressures, and takes a value near 4.5 for $P_0/P_t = 50$ (*19*). As the fluid-rock mixture is expected to have $c_0 \approx 100$ m/s in the conduit and V/A may be approximated with the length of the conduit, 1000 m, the duration of the flow would be 40 to 50 s, which is close to the observed values. The temperature below the crater at Aso is poorly known, but the above scenario would be rather insensitive to the details of temperature profiles.
22. The large SPT amplitudes and long duration for the large eruptions can be qualitatively interpreted in the framework of the choked flow model. If fluid-rock mixtures flow not only from the conduit but also out of the reservoir itself, the volume-orifice ratio (V/A) should be effectively larger, and the duration is correspondingly longer. When the fluid-rock mixture deeper in the reservoir is tapped, it naturally gains a larger excess pressure at the bottom of the cap rocks, resulting in a larger mass flow rate, which changes as AP_0/c_0 (*19*), corresponding to a larger SPT amplitude.
23. T. Gold and S. Soter, *Pure Appl. Geophys.* **122**, 492 (1985).

24. We thank Aso meteorological station for allowing us to deploy our instruments at its observation sites and for providing various data on the surface activity of Aso volcano. B. Chouet provided helpful comments on an earlier version of the manuscript. R. J. Geller critically reviewed the manuscript.

27 November 1995; accepted 10 June 1996

Impairment of Hippocampal Mossy Fiber LTD in Mice Lacking mGluR2

Mineto Yokoi, Katsunori Kobayashi, Toshiya Manabe, Tomoyuki Takahashi, Isako Sakaguchi, Goro Katsuura, Ryuichi Shigemoto, Hitoshi Ohishi, Sakashi Nomura, Kenji Nakamura, Kazuki Nakao, Motoya Katsuki, Shigetada Nakanishi*

Subtype 2 of the metabotropic glutamate receptor (mGluR2) is expressed in the presynaptic elements of hippocampal mossy fiber–CA3 synapses. Knockout mice deficient in mGluR2 showed no histological changes and no alterations in basal synaptic transmission, paired-pulse facilitation, or tetanus-induced long-term potentiation (LTP) at the mossy fiber–CA3 synapses. Long-term depression (LTD) induced by low-frequency stimulation, however, was almost fully abolished. The mutant mice performed normally in water maze learning tasks. Thus, the presynaptic mGluR2 is essential for inducing LTD at the mossy fiber–CA3 synapses, but this hippocampal LTD does not seem to be required for spatial learning.

Long-lasting modifications in synaptic efficacy at the mossy fiber–CA3 synapses in the hippocampus result from changes in presynaptic cells (*1–4*). In situ hybridization analysis and mGluR2 immunostaining after dentate gyrus lesion indicated that mGluR2 is predominantly expressed in dentate gyrus granule cells (*5*) and selectively distributed to mossy fibers (*6*). By contrast, mGluR2 is absent from the Schaffer collateral-commissural fiber–CA1 synapses (*5, 6*). Furthermore, immunoelectron micros-

Mechanism of Phreatic Eruptions at Aso Volcano Inferred from Near-Field Broadband Seismic Observations

Satoshi Kaneshima, Hitoshi Kawakatsu, Hirotoshi Matsubayashi, Yasuaki Sudo, Tomoki Tsutsui, Takao Ohminato, Hisao Ito, Koichi Uhira, Hitoshi Yamasato, Jun Oikawa, Minoru Takeo and Takashi Iidaka

Science **273** (5275), 642-645.
DOI: 10.1126/science.273.5275.642